Cancer & Metabolism

RESEARCH Open Access

Metabolism of primary high-grade serous ovarian carcinoma (HGSOC) cells under limited glutamine or glucose availability

Daniela Šimčíková[1], Dominik Gardáš[1], Tomáš Pelikán[1], Lukáš Moráň[2,3], Martin Hruda[1,4], Kateřina Hložková[5], Tiziana Pivetta[6], Michal Hendrych[7,8], Júlia Starková[5,9], Lukáš Rob[1,4], Petr Vaňhara[2,10] and Petr Heneberg[1*]

Abstract

Background High-grade serous ovarian carcinoma (HGSOC) is the most common and aggressive subtype of epithelial ovarian carcinoma. It is primarily diagnosed at stage III or IV when the 5-year survival rate ranges between 20% and 40%. Here, we aimed to validate the hypothesis, based on HGSOC cell lines, that proposed the existence of two distinct groups of HGSOC cells with high and low oxidative phosphorylation (OXPHOS) metabolism, respectively, which are associated with their responses to glucose and glutamine withdrawal.

Methods We isolated and cultivated primary cancer cell cultures from HGSOC and nontransformed ovarian fibroblasts from the surrounding ovarium of 45 HGSOC patients. We tested the metabolic flexibility of the primary cells, particularly in response to glucose and glutamine depletion, analyzed and modulated endoplasmic reticulum stress, and searched for indices of the existence of previously reported groups of HGSOC cells with high and low OXPHOS metabolism.

Results The primary HGSOC cells did not form two groups with high and low OXPHOS that responded differently to glucose and glutamine availabilities in the cell culture medium. Instead, they exhibited a continuum of OXPHOS phenotypes. In most tumor cell isolates, the responses to glucose or glutamine withdrawal were mild and surprisingly correlated with those of nontransformed ovarian fibroblasts from the same patients. The growth of tumor-derived cells in the absence of glucose was positively correlated with the lipid trafficking regulator *FABP4* and was negatively correlated with the expression levels of *HK2* and *HK1*. The correlations between the expression of electron transport chain (ETC) proteins and the oxygen consumption rates or extracellular acidification rates were weak. ER stress markers were strongly expressed in all the analyzed tumors. ER stress was further potentiated by tunicamycin but not by the recently proposed ER stress inducers based on copper(II)-phenanthroline complexes. ER stress modulation increased autophagy in tumor cell isolates but not in nontransformed ovarian fibroblasts.

Conclusions Analysis of the metabolism of primary HGSOC cells rejects the previously proposed hypothesis that there are distinct groups of HGSOC cells with high and low OXPHOS metabolism that respond differently to glutamine or glucose withdrawal and are characterized by ETC protein levels.

*Correspondence:
Petr Heneberg
petr.heneberg@lf3.cuni.cz

Full list of author information is available at the end of the article

Keywords Epithelial ovarian carcinoma, Metabolism reprogramming, Ovarian fibroblasts, Oxidative phosphorylation, Patient-derived cells, Unfolded protein response

Background

High-grade serous ovarian carcinoma (HGSOC) is the most common and aggressive subtype of epithelial ovarian carcinoma (OC) [1]. Most women are diagnosed at stage III or IV when the 5-year survival rate ranges between 20% and 40% [2]. The survival rate of HGSOC patients has not improved since the 1970s. The typical first-line treatment for advanced OC consists of surgical reduction of the tumor mass, followed by multiple cycles of paclitaxel and carboplatin or PARP inhibitors (for BRCA1/2 mutation carriers). Three chemotherapy cycles may be administered before surgery [3]. The response of HGSOC to chemotherapy has been suggested to be closely linked to the metabolic phenotype of the respective cancer case [4]. Typically, HGSOCs prioritizing oxidative phosphorylation (OXPHOS) over aerobic glycolysis exhibited a better response to chemotherapy [4].

Compared with cells of normal ovarian tissue, HGSOC cells express high levels of the endoplasmic reticulum (ER) stress-associated proteins GRP78, PERK, and ATF6. High expression levels of GRP78 and PDI are associated with poor survival, HGSOC aggressiveness, and disease progression [5, 6]. Additionally, TUSC3, an ER stress regulator responsible for the N-linked glycosylation of proteins in the endoplasmic reticulum, is strongly associated with the overall and disease-free survival of OC patients [7] and with the viability, epithelial–mesenchymal transformation, and migration of OC cells [8]. ER stress initiates a cascade of unfolded protein response (UPR) reactions. The UPR is linked to the progression of multiple cancer types [9]. In the normal ovarian epithelium, the UPR is periodically activated during follicular growth and maturation [10] and is further increased when the uterine lining is atrophied in menopausal women and ovariectomized animals [11]. One mechanism of UPR activation in OC cells involves PTEN loss, which drives constitutive mTORC1 activity and UPR induction; the mTORC1 and UPR signaling pathways are correlated in primary carcinoma samples [12]. ER stress can be pharmacologically induced by tunicamycin, which causes the accumulation of unfolded glycoproteins in the ER and is inhibited by salubrinal, which also acts as an autophagy activation inhibitor. Recently, the cytotoxicity of copper(II)-phenanthroline complexes was linked to ER stress modulation in OC cell lines [13, 14].

The acquired resistance of HGSOC to platinum-based chemotherapies is a critical issue. The UPR is involved in paclitaxel resistance independent of the antimitotic effects of taxanes [15] and is generally involved in cancer drug resistance [16–18]. Additionally, strong evidence has shown the role of cellular stress in the maintenance of senescent cisplatin-resistant HGSOC cells. Cisplatin induces substantial oxidative stress, which affects central carbon metabolism and upregulates NAD^+-dependent histone deacetylases, such as SIRT2; these prime HGSOC for cisplatin sensitivity [19, 20]. NAD^+ biosynthesis regulates the acquisition of the cisplatin-induced senescent phenotype in HGSOC [21], likely through NAMPT modulation [22]. The mechanism of action of some novel OC therapeutics, such as AZD1775, appears to be related to the induction of ER stress [23]. Other therapeutics, such as gonadotropin-releasing hormone analogs, protect ovarian function by relieving ER stress and modulating mTOR signaling and autophagy induction [24]. Metformin can also induce the UPR and autophagy in OC cells (but not normal ovarian epithelial cells), and the combination of autophagy and PERK activation protects OC cells against metformin-induced apoptosis [25]. Despite these findings, a direct link between ER stress and chemotherapy resistance in HGSOC remains to be determined.

Two distinct subgroups of HGSOC cell lines with high and low OXPHOS were previously reported [4]. These subgroups respond differently to chemotherapy and depletion of glucose or glutamine and are characterized by prominent differences in electron transport chain (ETC) protein expression [4]. Therefore, we hypothesized that these two groups of cells should be detectable in primary cancer cell isolates from HGSOC patients and that this classification should predict the spectrum of functional responses to ER stress modulation, pharmacotherapeutic targeting of cellular metabolism, and depletion of glucose or glutamine.

Materials and methods

Patients

Resected anonymized HGSOC tissues and matched normal adjacent ovarian tissues were obtained from Czech patients who underwent surgery for clinical purposes at the University Hospital Královské Vinohrady. Immediately after surgery, small pieces of tissue from selected patients were fixed in 4% neutral-buffered paraformaldehyde for further immunohistopathological examination. The remainder of the tissue was minced, cleaved by dispase, passed through a 100 µm strainer, and allowed to proliferate in 2D culture for two to six weeks [26]. The purity of the cultured cells was tested by staining single-cell-gated cells with the following antibodies: anti-vimentin-Alexa Fluor 488 (Cell Signaling Technology, Danvers, MA, #9854), anti-pan-keratin-PE (Cell

Signaling Technology, #5075), and anti-smooth muscle actin-Alexa Fluor 488 (eBioscience, San Diego, CA, #53-9760-82). The identity of randomly selected tumor cell isolates from patients with HGSOC of FIGO stage IIIC or higher was also confirmed by semiquantitative analysis of p53 expression (stained using DO-7, 1:200; Agilent DAKO) in formalin-fixed, paraffin-embedded blocks containing the cultured cells. The cells from matched normal adjacent tissues consisted of fibroblasts instead of the already mostly atrophied epithelia. The use of resected tissues was approved by the Ethics Committee of the Third Faculty of Medicine, Charles University (approval not numbered, dated April 29, 2020) and by the Ethics Committee of the University Hospital Královské Vinohrady (approval #EK-VP/24/0/2020, dated June 3, 2020). The clinical parameters of the examined cohort of patients are provided in Table S1.

The cells were cultivated at 37 °C in 5% CO_2. Mycoplasma contamination was routinely assessed by qPCR (Eurofins Genomics, Ebersberg, Germany). DMEM (Thermo Fisher Scientific; Gibco #A14430-01) supplemented with or without 5.5 mM glucose and/or 2 mM glutamine and 10% FBS was used unless otherwise stated. The FBS contained 4 mM glucose and ~1 mM glutamine; therefore, the final glucose concentration in the glucose-depleted medium was 0.4 mM, and the final glutamine concentration in the glutamine-depleted medium was ~0.1 mM.

ER stress modulation

We used Western blotting to examine the expression of key ER stress regulators in seven primary cell cultures isolated from HGSOC and in five fibroblast isolates from the surrounding ovarium. Specifically, we determined the levels of BiP, P-eIF2α (S51), and total eIF2α. We also analyzed P-PERK (T982) and total PERK in nontransformed fibroblasts. We modulated the levels of ER stress with the following compounds: the prototypic ER stress inducer tunicamycin, two other previously suggested ER stress inducers consisting of copper(II)-phenanthroline complexes containing different imidazolidine-2-thione ligands (the complexes were designated as C0 and C1 as specified below), salubrinal alone or in combination with C1 as a compound that alleviates ER stress, and tauroursodeoxycholic acid (TUDCA). Tunicamycin, salubrinal, and TUDCA were obtained from Sigma–Aldrich (St. Louis, MO); C0 and C1 were synthetized as described [27]. The modulation of ER stress by the two mixed copper(II)-phenanthroline complexes was previously shown to induce the UPR in OC cell lines [13, 14]. These consisted of the parental compound $[Cu(phen)_2(OH_2)](ClO_4)_2$ (designated as C0); and a complex that was previously synthesized from the parent complex, namely, $[Cu(phen)_2(2\text{-imidazolidinethione})](ClO_4)_2$ (designated as C1) [27]; in some cases, we administered C1 together with salubrinal.

Histopathological examination

A histopathological examination was performed to measure the ER stress levels and confirm the identity of the examined tissues. We performed immunohistochemical staining of tissues fixed in 4% buffered paraformaldehyde (Santa Cruz Biotechnology, Dallas, TX), washed in PBS, dehydrated in an Autotechnicon tissue processor, and embedded in paraffin blocks. Five-micrometer-thick tissue sections were deparaffinized in xylene and rehydrated in ethanol. Antigen retrieval was performed using a Target Retrieval Solution at pH 6 or 9 (Dako, Jena, Germany) for 30 min at 98 °C, which was followed by treatment with 0.3% H_2O_2 in PBS (pH 7.4) to quench endogenous peroxidase activity. Blocking was performed by incubating the sections with 10% BSA for 30 min, after which they were incubated with the primary antibody for one hour at room temperature. The primary antibodies were diluted in Antibody Diluent (Dako, Jena, Germany). The sections were then incubated with the biotinylated antibody reagent DAKO EnVisionTM+Dual Link (Dako, Jena, Germany) for 20 min at room temperature. Finally, the sections were incubated with streptavidin-HRP (LSAB1System HRP, Dako, Germany) until a brown color developed. The sections were then counterstained with Gill's hematoxylin, dehydrated, and mounted with Pertex medium. The list of primary antibodies used and the reaction conditions are provided in Table S2. The expression of E-cadherin and N-cadherin was assessed by a semiquantitative scoring system. E-cadherin expression was scored as follows: 0, no immunoreactivity; 1+, incomplete or dot-like faintly membranous immunoreactivity; 2+, complete circumferential membranous immunoreactivity of <10% of the cells; and 3+, complete circumferential membranous immunoreactivity of ≥10% of the cells. The expression of other markers, namely PERK, eIF2α, vimentin, calnexin, CHOP, and BiP was evaluated on a scale from 0 to 3: 0, negative; 1, detectable but weak; 2, moderate but submaximal; and 3, maximal.

Flow cytometry

We analyzed the uniformity of the adherently grown primary cells isolated from HGSOC tumors (designated as tumor cells) and the adherently grown nontransformed primary fibroblasts from the surrounding ovarium (designated as fibroblasts) by flow cytometric analysis of pan-keratin, α-actin, and vimentin expression. The cells were trypsinized, permeabilized three times for 5 min each time with 0.1% Triton X-100 in PBS, blocked for 30 min with 5% BSA in PBS, and stained with the antibodies anti-pan-keratin-PE (Cell Signaling Technology, clone C11) and

anti-α-actin-Alexa Fluor 488 (eBioscience, clone 1A4) or anti-vimentin-Alexa Fluor 488 (Cell Signaling Technology, clone D21H3) in 5% BSA for 1 h at room temperature. The cells were washed three times with 0.1% Triton X-100 in PBS and stored in PBS supplemented with 0.02% azide until analysis with a FACSVerse (Becton Dickinson, Franklin Lakes, NJ).

Assays for cell viability, proliferation, and redox status

We measured cell viability in 96-well plates with the alamarBlue cell viability reagent (Thermo Fisher Scientific, Waltham, MA) according to the manufacturer's instructions. We also indirectly assessed changes in cell counts by measuring ATP levels with CellTiter-Glo (Promega, Madison, WI) according to the manufacturer's instructions. We also determined cell proliferation by counting trypan blue-stained cells. All measurements were obtained from three or more independent experiments, each performed in quadruplicate.

We further evaluated a randomly selected set of isolates of tumor cells for changes in reactive oxygen species (using CM-H_2DCFDA at 1.6 μg mL^{-1}, with an excitation at 493±20 nm and an emission at 520±20 nm), mitochondrial superoxide (using 1 μM MitoSOX Red, with an excitation at 396±20 nm and an emission at 610±20 nm), and intracellular reduced glutathione (using 10 μM ThiolTracker Violet, with an excitation at 405±20 nm and an emission at 526±20 nm) (all from Thermo Fisher Scientific, Waltham, MA) according to the manufacturer's instructions. The compounds were diluted in phosphate-buffered saline and incubated for 20 min. Following these measurements, we lysed the cells in CellTiter-Glo and transferred the lysates to white plates for endpoint ATP measurements. The measurements were performed with a Spark microplate reader (Tecan, Männedorf, Switzerland).

RNA isolation, qRT–PCR and immunoblotting

We isolated RNA with a PicoPure RNA isolation kit (Applied Biosystems, Waltham, MA). We transcribed the isolated RNA with a SuperScript VILO cDNA synthesis kit (Invitrogen, Waltham, MA) and performed qRT–PCR with the 7500 Fast Real–Time PCR System (Applied Biosystems). We used GAPDH for normalization in all the experiments. We assessed mRNA expression with TaqMan probes (Table S3) and TaqMan Fast Advanced Master Mix (all from Thermo Fisher Scientific). All measurements were performed in triplicate.

For Western blotting, we used NuPAGE Bis-Tris 4 to 12% mini protein gels and NuPAGE MES SDS Running Buffer (both from Thermo Fisher Scientific). We quantified the Western blots with ImageLab (Bio-Rad Laboratories, Hercules, CA). The list of primary antibodies used for Western blotting is provided in Table S4. The uncropped blots are provided in Supplementary File 2.

Extracellular acidification rate (ECAR)

Glycolytic parameters were measured using the Glycolysis Stress Test on a Seahorse Analyzer XFp (Agilent Technologies, Santa Clara, CA). The cells were plated at a density of 2×10^4 cells per well in XFp tissue culture plates. The next day, the cell monolayers were washed and incubated for 30 min in XF Base Medium, pH 7.4. Before performing the measurements, the cells were counted using a SpectraMax i3 (Molecular Devices, San Jose, CA). The following compounds were sequentially injected at 10× concentrations to reach the following final concentrations: 10 mM glucose, 2 μM oligomycin A, and 100 mM 2-deoxyglucose. At least three biological replicates and five technical replicates were measured for each patient.

Oxygen consumption rate (OCR)

Mitochondrial respiration parameters were measured using the Cell Mito Stress Test on a Seahorse Analyzer XFp (Agilent Technologies). The cells were plated at a density of 2×10^4 cells per well in XFp tissue culture plates. The next day, the cell monolayers were washed and incubated for 30 min in XF Assay Medium, pH 7.4, supplemented with 10 mM glucose, 1 mM HEPES, pH 7.4, 1 mM pyruvate, and 0.1% BSA. Before performing the measurements, the cells were counted using a SpectraMax i3 (Molecular Devices). The following compounds were sequentially injected at 10× concentrations to reach the following final concentrations: 2 μM oligomycin A, 0.5 μM and 1.0 μM FCCP (sequentially), and 1 μM rotenone combined with 1 μg/ml antimycin A. At least three biological replicates and five technical replicates were measured for each patient.

Statistical analysis

All the measurements were obtained from three or more independent experiments. The data are shown as the means±SEs unless stated otherwise. The Spearman correlation coefficient was used to estimate associations between continuous variables. Student's *t*-test, the REML mixed-effect model followed by Tukey`s multiple comparison tests, and one-way ANOVA with the Student–Newman–Keuls post-hoc tests were used for the statistical analyses. All the data were tested for equality of variance and distribution normality; if the data did not fulfill these conditions, Kruskal–Wallis ANOVA with Dunn's post-hoc tests was used. The statistical analyses were conducted in SigmaPlot 12.0 (Systat Software, San Jose, CA) or GraphPad Prism 8 (Dotmatics, Boston, MA). Differences were considered statistically significant at $p<0.05$.

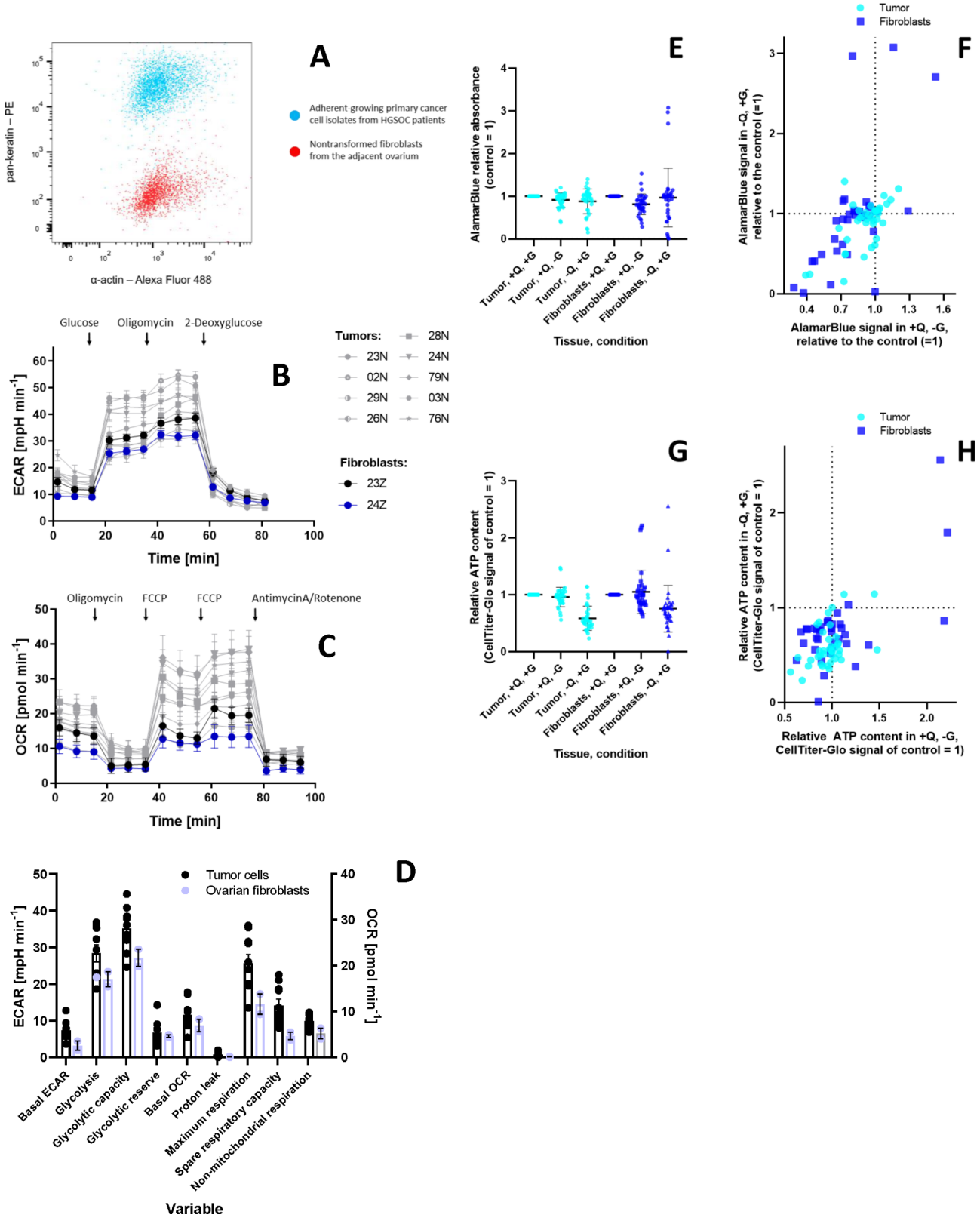

Fig. 1 (See legend on next page.)

(See figure on previous page.)

Fig. 1 Characterization of primary cell cultures. (**A**) Example of the FACS analysis of tumor cells (blue) and ovarian fibroblasts (red) according to their α-actin (PE) and pan-keratin (Alexa Fluor 488) expression. (**B-D**) Differences in the ECAR (**B**) and OCR (**C**) among tumor cells ($n=9$; shown in grey) and ovarian fibroblasts ($n=2$; shown in color). (**D**) Basal ECAR, glycolysis, glycolytic capacity, glycolytic reserve, basal respiration, proton leakage, maximum respiration, spare respiratory capacity, and non-mitochondrial respiration in tumor cells and ovarian fibroblasts. (**E-H**) Resazurin reduction rates and cellular ATP levels. Relative absorbances of alamarBlue (**E-F**) and CellTiter-Glo (**G-H**) in tumor cells (tumor) and ovarian fibroblasts (fibroblasts) cultivated in complete medium (+Q, +G) or medium with depleted glucose (+Q, -G) or glutamine (-Q, +G). Individual data points represent the means of four measurements from each patient-derived cell isolate and are shown relative to those of the isolates in complete medium (+Q, +G). The bars indicate the means and SDs (**B, C,E, G**) or SEs (**D**). Asterisks (*) indicate significant differences at $\alpha < 0.05$ in the REML mixed-effect model, followed by Tukey`s multiple comparison tests

Results and discussion

Metabolic activity of tumor cells and ovarian fibroblasts

After several passages, the cells exhibited uniform patterns. They were depleted of stroma and adipocytes and lost abundant lipid droplets within the first few days of culture. Tumor cells were positive for pan-keratin and α-actin (Fig. 1A). Most but not all tumor cell isolates stained strongly for p53, and the stains were uniform within individual cell isolates. These data combined suggest their epithelial origin and acquisition of mesenchymal features through epithelial–mesenchymal transition, and the uniform and mostly strong p53 stains confirm their identity as HGSOC isolates. Ovarian fibroblasts were positive for α-actin but negative for pan-keratin (Fig. 1A). Epithelial cells were lacking due to age-related changes in the ovarium, and these samples gave rise to uniform ovarian fibroblast populations.

The ECAR and OCR were generally greater for tumor cells than ovarian fibroblasts (Fig. 1B-D). The most prominent differences were in basal ECAR (one-tailed t-test $p=0.03$), maximum respiration (one-tailed t-test $p=0.04$), spare respiratory capacity (one-tailed t-test $p=0.03$), and non-mitochondrial respiration (one-tailed t-test $p=0.02$) (Fig. 1D). However, the interindividual differences were prominent and we focused on their possible causes. In OC cell lines, increased respiratory capacity was previously correlated with OXPHOS activity and ETC protein levels. Importantly, these cells differed in their preferences for glucose or glutamine to fuel mitochondrial respiration [4].

Since data on glucose and glutamine preferences from primary tumor cells were lacking, we measured the redox state employing the resazurin reduction rate and cellular ATP by CellTiter-Glo in media supplemented with glucose and glutamine or with either glucose or glutamine alone. We found that the resazurin reduction rate decreased in most (but not all) tumor cell isolates following the depletion of glucose or glutamine (Fig. 1E). In ovarian fibroblasts, these decreases were present in most glucose-deprived cells but in only a few glutamine-deprived isolates (Fig. 1E). Therefore, in tumor cells, the resazurin reduction rates of glucose-deprived and glutamine-deprived cells were predominantly correlated with each other. However, a subgroup of tumor cell isolates (only ~ 10% of the total) that displayed restricted metabolism under glutamine-deprived but not glucose-deprived conditions was also observed (Fig. 1F). In most tumor cell isolates, the responses to glucose or glutamine withdrawal were mild.

The ATP measurements revealed no differences in cell number following glucose depletion in either tumor cells or ovarian fibroblasts (Fig. 1G). For six randomly selected tumor cell isolates, we matched the data from the cell ATP measurements with the data from trypan-blue-based cell counting; these results suggested a good agreement between the methods used (Fig. S1). Taken together, these data suggested that both cell types exhibited lower resazurin reduction rates following glucose depletion (Fig. 1E). In contrast, glutamine depletion induced prominent decreases in ATP levels in wells with both tumor cells and ovarian fibroblasts (Fig. 1G). This finding is consistent with the role of glutamine as an important ATP source. Glutamine is likely more important than glucose as an ATP source because glutamine allows ATP generation by entering the Krebs cycle via glutamate and α-ketoglutarate. The decreases in ATP levels in wells with cells cultured in glucose- and glutamine-depleted media were not correlated (Fig. 1H). The relatively uniform pattern of the response to glucose and glutamine withdrawal was surprising, given that previously published data from OC cell lines suggested the existence of differentially responsive populations [4]. Previously reported differences in OXPHOS rates and addiction to glucose or glutamine may represent artifacts of long-term cell culture. The adverse effects of long-term cell culture can also be deduced from the more prominent effects of glutamine withdrawal relative to glucose withdrawal, as many long-term cultivated cells become glucose-addicted even though they were initially glutamine-addicted [28–30]. Glucose-addicted tumor cells are sensitive to chemotherapy, whereas glucose-deprivation-resistant tumor cells are resistant to chemotherapy [31, 32].

The study design provided a great opportunity to analyze matched tumor cells and ovarian fibroblasts from the same patient. Surprisingly, patient-specific responses of tumor cells and ovarian fibroblasts were correlated with one another following the depletion of glucose or glutamine. A strong negative correlation was also observed between the proliferation of ovarian fibroblasts following the withdrawal of glutamine and the proliferation of tumor cells from the same patients, as measured in the

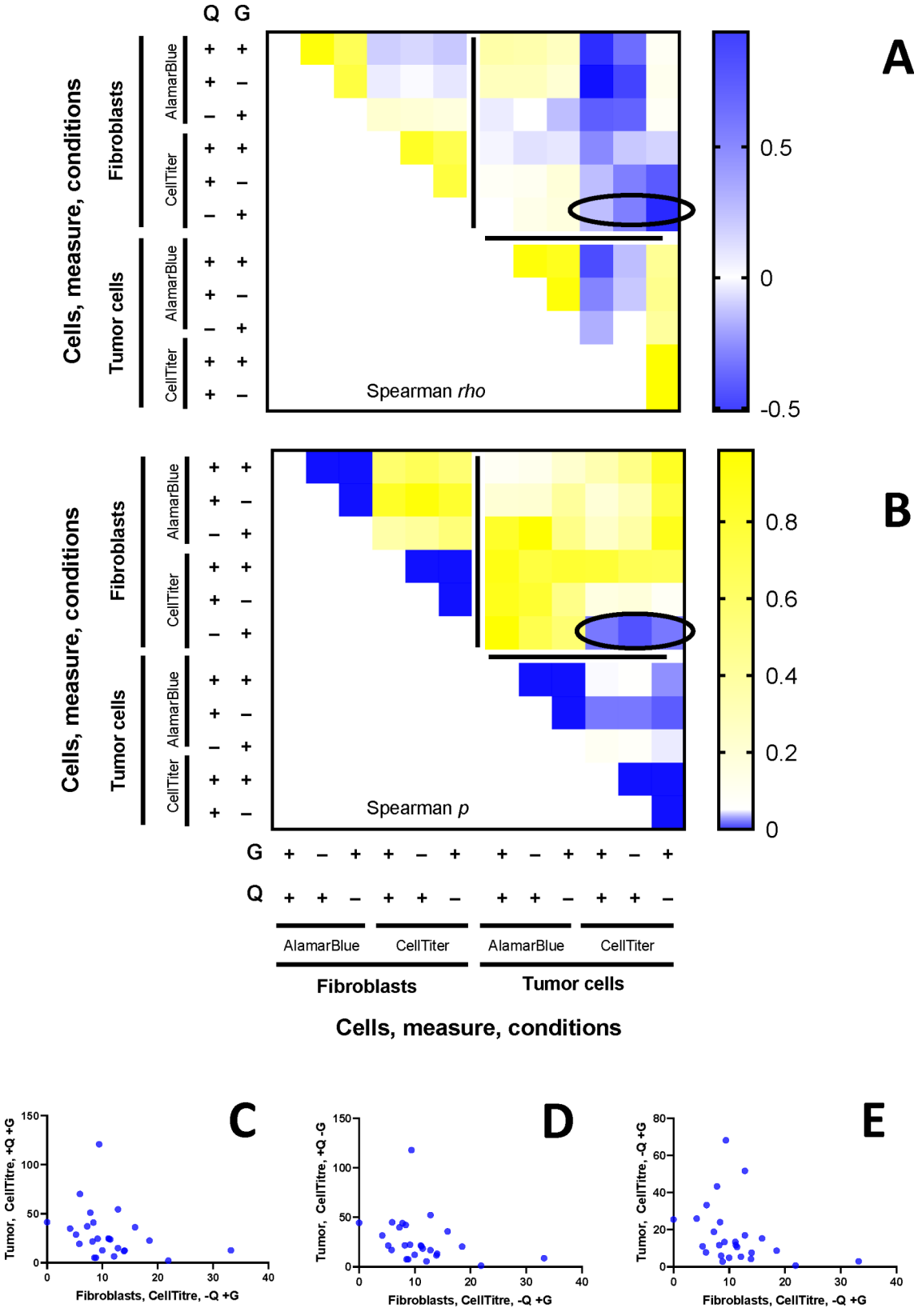

Fig. 2 (See legend on next page.)

(See figure on previous page.)

Fig. 2 Heatmap of the Spearman *rho* correlation analysis of the resazurin reduction rates and cellular ATP levels in matched tumor cells and ovarian fibroblasts from the same patient. The data are shown for the alamarBlue and CellTiter-Glo measurements analyzed as absolute values (relative to the cell count) for tumor cells (tumor) and ovarian fibroblasts (fibroblasts) cultivated in complete medium (+Q, +G) or in medium with depleted glucose (+Q, -G) or glutamine (-Q, +G). (**A**) Spearman *rho* values. (**B**) Spearman *p* values. The correlations in (**A**) compared data obtained from the tumors (lower right quadrant) and fibroblasts (upper left quadrant) and compared the values obtained from matched patient isolates of the two cell types (upper right quadrant). The ovals indicate significant negative correlations for which individual data points are shown in (**C-E**). (**C-E**) Dot plots of CellTiter-Glo values for cancer cells cultivated in +Q, +G medium (**C**), +Q, -G medium (**D**), and -Q, +G medium (**E**) compared with CellTiter-Glo values for ovarian fibroblasts from paired patient-specific samples cultivated in -Q, +G medium. The data in (**C-E**) were calculated relative to the number of cells present prior to the addition of the specific cell culture media

presence of both glucose and glutamine or the presence of only one of these compounds (Fig. 2). The resazurin reduction rate did not reveal such correlations (Fig. 2).

Gene and protein expression patterns

Genes involved in regulating glycolysis and glutamine metabolism were previously suggested to be predictors of the OXPHOS activity of HGSOC cell lines [4]. Therefore, we analyzed the transcript levels of 14 genes involved in metabolic pathways, particularly those involved in regulating glycolysis and glutamine metabolism (Fig. S2). The proliferation of tumor cells in the absence of glucose was negatively correlated with the expression levels of *HK2* and *HK1*. Notably, the expression of transcripts of these two hexokinase isoforms was correlated with one another (Spearman $rho=0.65$; $p<0.001$). In contrast, the proliferation of tumor cells in the absence of glucose was positively correlated with the expression levels of lipid trafficking regulator *FABP4*, which is known to be upregulated in various malignant solid tumors and is correlated with a poor prognosis [33, 34]. In the absence of glutamine, the proliferation of tumor cells was negatively correlated with the expression levels of *HK2* (but not those of *HK1*, which is more abundant in these cells; see [35]) (Fig. S2).

With respect to ovarian fibroblasts, we analyzed the expression of only four genes, *HK1*, *HK2*, *IDO1*, and *SLC7A11*. Similar to the findings in tumor cells, we found a positive correlation between *HK1* and *HK2* expression in ovarian fibroblasts. In addition, we detected a positive correlation between *IDO1* expression and alamarBlue readouts in cells grown in media supplemented with both glutamine and glucose or with glucose alone (Fig. S2A). When we compared the levels of these four transcripts (*HK1*, *HK2*, *IDO1*, and *SLC7A11*) in tumor cells and corresponding ovarian fibroblasts in patient-matched samples, we detected no correlation between their expression in ovarian fibroblasts and that in patient-matched tumor cells (Fig. S2C).

At the protein level, HGSOC cell lines with high and low OXPHOS rates are characterized by prominent differences in ETC protein expression [4]. The correlations of CellTiter-Glo readouts of tumor cells grown in glucose- or glutamine-deficient media with the expression of ETC proteins were weak (Spearman $p>0.05$ for all correlations between ETC II, III, IV, and V compared to ATP levels in wells with tumor cells grown in glucose-deficient or glutamine-deficient media). An overview of patient-matched data is shown in Fig. 3A, where the tumor cell isolates are sorted according to the ATP levels detected after cultivation in glutamine-deficient media. Similarly, OCR or ECAR parameters were mostly independent on the expression of ETC proteins. The only significant correlations for ECAR were when basal ECAR was compared to ETC IV expression (Spearman $rho=-0.63$, $p=0.04$). The only significant correlations for OCR were when spare respiratory capacity was compared to ETC IV expression (Spearman $rho=-0.61$, $p=0.03$) and when non-mitochondrial respiration was compared to ETC II and ETC V expression (Spearman $rho=0.81$, $p=0.004$ and $rho=0.596$, $p=0.04$, respectively). An overview of patient-matched data is shown in Fig. 3B, where the tumor cell isolates are sorted according to the ETC IV expression levels. Importantly, tumor cells did not form two distinct clusters when stratified according to their expression of ETC proteins, cellular proliferation, metabolic activity, mitochondrial respiration, or glycolytic activity (Figs. 1 and 3).

Metformin and erastin

The viability of high-OXPHOS cell lines is selectively inhibited by metformin [4]. Metformin, an inhibitor of mitochondrial complex I, reportedly affects the viability of high-OXPHOS cells but not that of low-OXPHOS cells [4]. To inhibit the mitochondrial respiratory chain directly, previous studies have typically used up to 5 mM metformin in vitro [4, 36, 37], which leads to a compensatory increase in glycolysis [38, 39]. In our previous study of ovarian cancer cell lines, we used 2 mM and 10 mM metformin, with somewhat different effects observed at the two concentrations [35]. We titrated the effects of metformin (0.2–10.0 mM) on three randomly selected isolates of tumor cells (in complete medium and media without glucose or glutamine) with an alamarBlue assay. We found that one of the tumor cell isolates was unresponsive, one responded partially to 5 mM and 10 mM metformin in the glucose-depleted medium, and the alamarBlue signal was eliminated by 5 mM and 10 mM metformin in the glucose-depleted medium in the third tumor cell isolate (Fig. S3). Therefore, we used 2 mM

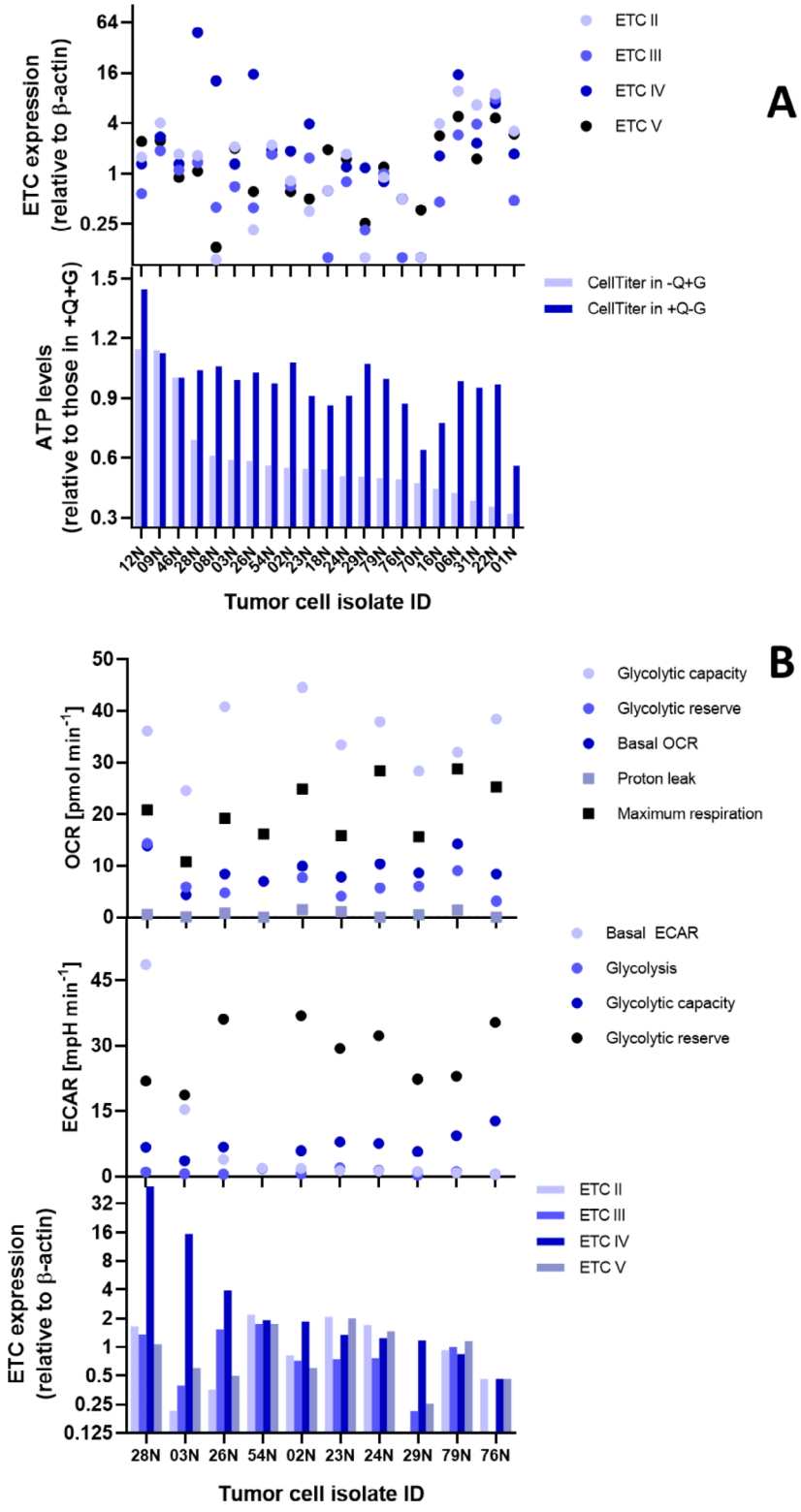

Fig. 3 The lack of two distinct clusters among tumor cell isolates stratified according to their proliferation (indirectly assessed by ATP levels) in glucose-deficient and glutamine-deficient media, expression of ETC proteins, ECAR, and OCR. (**A**) An overview of patient-matched data of CellTiter-Glo readouts of tumor cells grown in glucose- or glutamine-deficient media (lower part of the subfigure) compared with the expression of ETC proteins (upper part of the subfigure). The tumor cell isolates are sorted according to the ATP levels detected after cultivation in glutamine-deficient media. (**B**) An overview of patient-matched data of the ETC protein expression (lower part of the subfigure) compared with ECAR (middle part of the subfigure) and OCR (upper part of the subfigure) parameters. The tumor cell isolates are sorted according to the ETC IV expression levels

and 10 mM metformin in the present study of primary isolates.

The OXPHOS status of tumor cells did not correlate with the response to metformin treatment (Fig. 4), and the differential metformin-induced reduction in high-OXPHOS cell viability, as opposed to the lack of impact on low-OXPHOS cells (both proposed on the basis of cell line data), was not recapitulated in tumor cells. Instead, the response to metformin was much more prominent in glucose-depleted cells.

We found that metformin alone induced only weak effects on the proliferation and metabolic activity of tumor cells. Notably, metformin combined with glutamine withdrawal, and particularly metformin combined with glucose withdrawal severely decreased the proliferation and metabolic activity of tumor cells (Fig. 4, Fig. S1). The ovarian fibroblasts were much more resistant to metformin treatment. Only the combination of metformin treatment with glucose withdrawal induced significant decreases in the proliferation and metabolic activity of these cells (Fig. 4, Fig. S4). Notably, while ATP measurements closely matched data from trypan blue-based cell counting in metformin-untreated cells, some isolates of tumor cells (Fig. S1) and one of the three tested isolates of ovarian fibroblasts (Fig. S4) presented decreases in ATP values that were disproportional to changes in number of cells. These differences were particularly prominent in the glucose-deprived medium (Fig. S1). The mechanistic explanation of the differential effects of metformin with or without glucose withdrawal stems from the blockade of complex 1 by metformin. ATP can still be generated by complex 2, which uses $FADH_2$. Therefore, glucose removal had cytotoxic effects as metformin-treated tumor cells lacked glycolysis-derived ATP. A glucose-depleted environment is characteristic of central parts of large or poorly vascularized tumors [40], where metformin could be more effective than previously thought on the basis of experiments in glucose-rich cell culture conditions.

The sensitivity to glutamine led us to test the effects of the xCT inhibitor erastin, which induces ferroptosis and is cytotoxic to some but not all OC cell lines [41–43]. The cystine–glutamate antiporter xCT is essential for the import of cystine into ovarian cancer cells. These cells use cystine for the intracellular synthesis of glutathione and for regulating the intracellular redox balance. In line with the above findings, ovarian cancer cells are often stimulated by high levels of cystine or glutathione itself from the tumor microenvironment [43]. Thus, xCT is crucial for the survival and maintenance of redox balance in ovarian cancer cells. However, whether any synergy exists between the shift in nutrient availability and the outcome of erastin treatment in TC remains unclear. The individual tumor cells and ovarian fibroblast isolates varied in their response to erastin alone. Compared with patient-matched ovarian fibroblasts, tumor cells were more sensitive to erastin treatment when evaluated by ATP measurements. But both of these cell types displayed an inhibition of metabolism. The withdrawal of glucose or glutamine did not affect the outcomes of erastin treatment (Fig. 4E-F).

ER stress in HGSOC and the adjacent ovary

The increased sensitivity of tumor cells to oxidative stress often leads to the onset of ER stress [44]. Immunohistochemical analysis of a subset of paraformaldehyde-fixed HGSOC tumors revealed that the tumor cells expressed high levels of ER stress markers, including BiP, PERK, eIF2α, CHOP, and calnexin (Fig. 5A-D; Fig. S5). CHOP staining was strong not only in tumor cells but also in infiltrating immune cells and, to a lesser extent, in other cells of the tumor microenvironment and in fibroblasts in the adjacent ovary. Nevertheless, all cells of the analyzed compartments were CHOP-positive. In contrast, the adjacent ovary tissue was negative for all other ER stress markers. Stromal cells were only weakly positive for ER stress markers. Infiltrating immune cells displayed a similar percentage of PERK- and eIF2α-positive cells as the tumor cells, but the percentages of BiP- and calnexin-positive cells were lower than those in corresponding tumor cells, which suggests that the ER stress pathways were not fully activated in infiltrating immune cells (Fig. 5A).

Owing to the high expression of ER stress markers in tumor cells, we treated a subset of tumor cells with TUDCA. This compound prevents UPR dysfunction and attenuates ER stress. In line with the above findings, TUDCA treatment led to increased proliferation of tumor cells cultivated in complete or glucose-deficient media (Fig. 5E). The responses of individual tumor cell isolates were heterogeneous, which suggests differences at the molecular level.

Therefore, we examined the protein expression of key ER stress regulators. All the examined primary cell isolates were susceptible to further increases in ER stress caused by tunicamycin but not copper(II)-phenanthroline complexes when evaluated by BiP expression (Fig. 5F-H; Fig. S6). This finding strongly contrasts with the data obtained previously in OC cell lines, namely, A2780 and SKOV-3 [13], and with reports of the generally cytotoxic effects of these compounds [13, 45]. These complexes have a strong affinity for DNA in vitro; however, the exact mechanism of their previously reported induction of the UPR in ovarian cancer cells remains unclear. The absence of an ER stress response following C0 and C1 treatments in primary cell cultures isolated from HGSOC was surprising, given that their cytotoxic effects were previously reported in the two abovementioned ovarian cancer cell

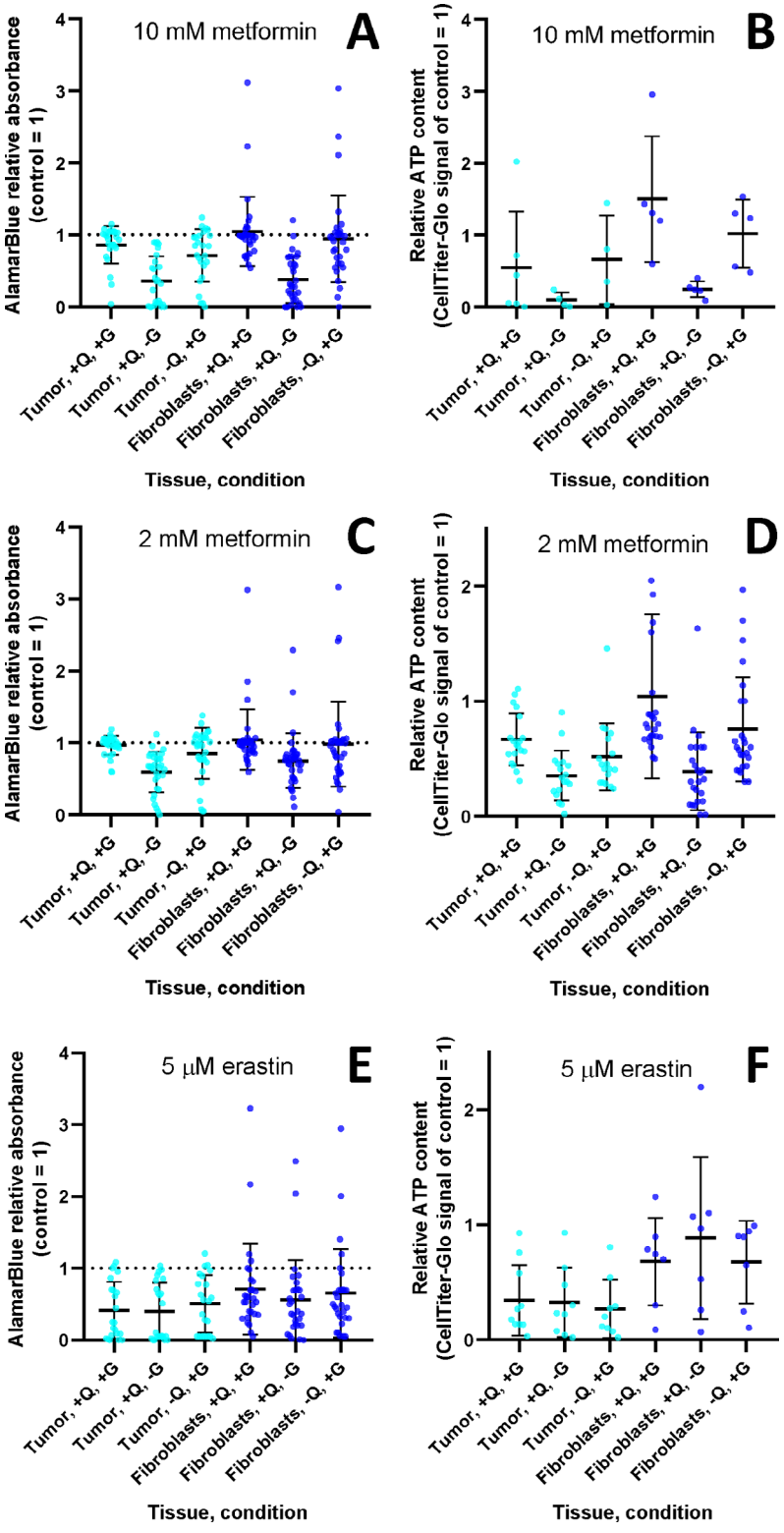

Fig. 4 Inhibition of the mitochondrial respiratory chain by high-dose metformin and xCT (SLC7A11) inhibition by erastin. The levels of resazurin reduction rates (**A, C, E**) and cellular ATP levels (**B, D, F**) following the incubation of cells with 10 mM metformin (**A, B**), 2 mM metformin (**C, D**) or 5 μM erastin (**E, F**). Relative absorbances of alamarBlue (**A, C, E**) and CellTiter-Glo (**B, D, F**) in tumor cells (tumor) and ovarian fibroblasts (fibroblasts) cultivated in complete medium (+Q, +G) or medium with depleted glucose (+Q, -G) or glutamine (-Q, +G). Individual data points represent the means of four measurements from each patient-derived cell isolate and are shown relative to those of the isolates in complete (control) medium (+Q, +G) without the study compound. The bars indicate the means and SDs

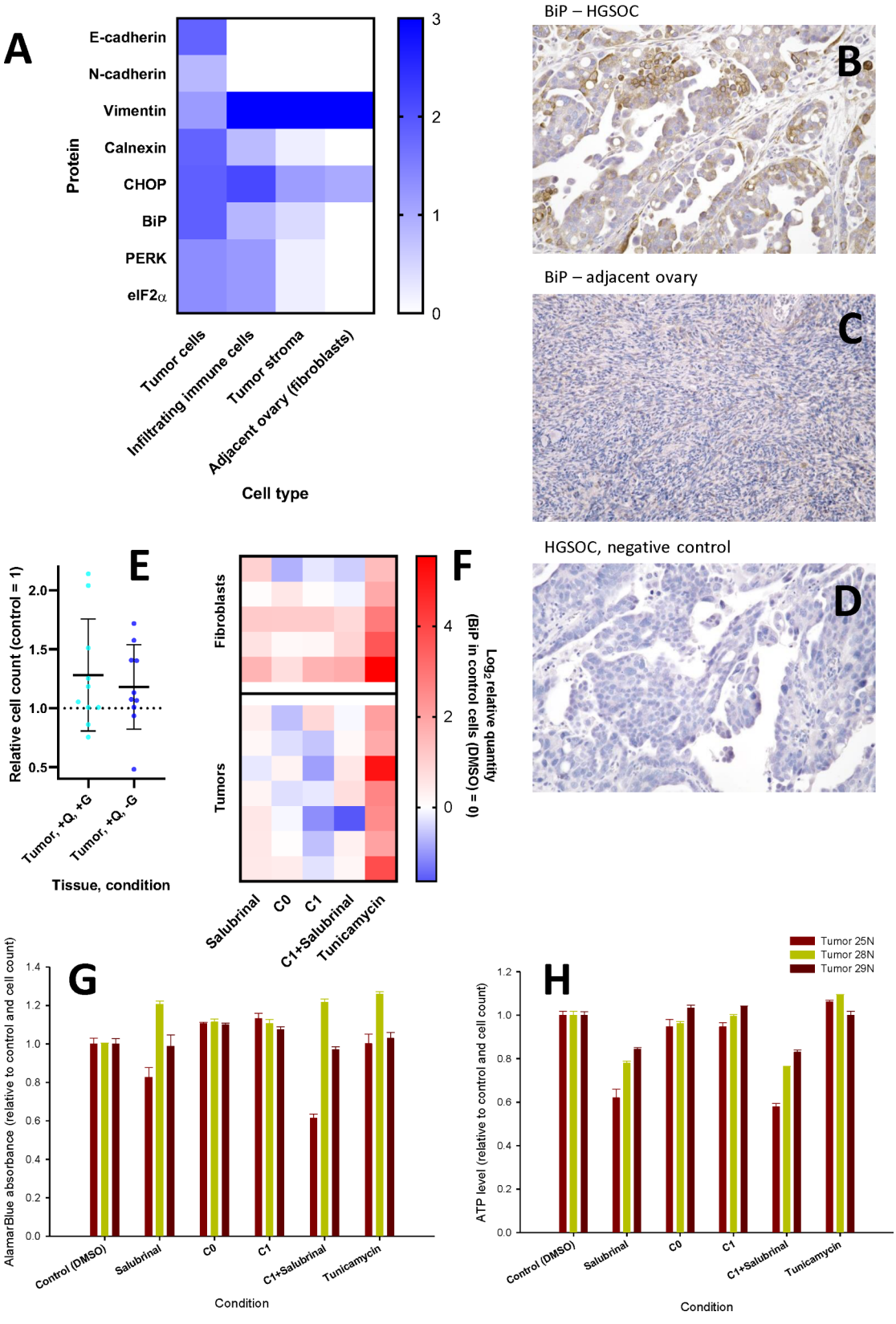

Fig. 5 (See legend on next page.)

(See figure on previous page.)

Fig. 5 ER stress in HGSOC and adjacent ovarian tissues. (**A**) Heatmap summarizing the outcomes of immunohistochemical staining of a subset of paraformaldehyde-fixed HGSOC tumors. The data are shown for the quantity of positive cells among cells of the indicated type. (**B, C, D**) Examples of immunohistochemical staining for BiP (200× magnification) in tumor tissue (**B**), and tissue from the adjacent ovary (**C**); a negative control of the tumor tissue is also provided (**D**). (**E**) Changes in the relative cell count of tumor cells (tumor) following incubation with TUDCA in complete medium (+Q, +G) or medium with depleted glucose (+Q, -G). (**F**) Changes in BiP levels following treatment with compounds that modulate ER stress. The tumor cells (tumor) and ovarian fibroblasts (fibroblasts) were incubated with DMSO (as a control), salubrinal, copper(II)-phenanthroline complexes C0 and C1, a mixture of C1 with salubrinal, or tunicamycin, and the protein expression of BiP was subsequently analyzed by Western blotting. The heatmap shows the relative expression levels of BiP in individual patients. The data are shown as log2 quantities relative to the DMSO control (0; white). Blue indicates decreased expression; red indicates increased expression. (**G-H**) Changes in the resazurin reduction rate and cellular ATP levels following treatment with compounds that modulate ER stress. The data are shown for the alamarBlue and CellTiter-Glo assay measurements, which were analyzed as values relative to those of tumor cells cultivated in a complete medium. The cells were incubated with DMSO (as a control), salubrinal, copper(II)-phenanthroline complexes C0 and C1, a mixture of C1 with salubrinal, or tunicamycin. The data from three independent tumor cell isolates, each measured four times, are shown

lines and other cancer cell lines [45]. Additionally, salubrinal alone or combined with C1 did not induce any major change in BiP expression in tumor cells or ovarian fibroblasts (Fig. 5F-H; Fig. S6). When eIF2α phosphorylation was examined, the data were more heterogeneous (Fig. S6; Fig. S7). The total level of PERK and its phosphorylation at T982 changed in the same direction (Fig. S8).

ER stress modulation increased autophagy in isolates of tumor cells but not in nontransformed fibroblasts

Under ER stress conditions, the UPR and ubiquitin–proteasome system often fail to restore the ER to its normal state when stimuli persist or are too strong. The damaged ER can be partially engulfed for degradation by autophagic vesicles when ER stress persists [46]. Therefore, we investigated autophagy markers to determine whether ER stress in primary cell cultures isolated from HGSOCs and fibroblasts from the surrounding ovarium was linked to an increased autophagic response. Specifically, we analyzed P-ULK1 (S757), total ULK1, P-AMPK (T172), and total AMPK levels, LC3B II/I ratios, and VPS34 levels.

The P-ULK1 (S757) / total ULK1 ratio in tumor cells but not in ovarian fibroblasts decreased following treatment with all of the tested ER stress-modulating compounds (Fig. S9; Fig. S10). The levels of total ULK1 varied, and the direction of responses to ER stress-modulating compounds depended on the initial ULK1 levels (Fig. S10); similar issues with interindividual variability were detected when the LC3B II/I ratio was measured (Fig. S9; Fig. S10). We also quantified the phosphorylation of AMPK at T172 as a proxy for the promotion of AMPK-mediated autophagy [47]. In tumor cells and ovarian fibroblasts, autophagy was not upregulated through T172 phosphorylation of AMPK (Fig. S9C-D). The responses of VPS34, an essential regulator of autophagosome generation, endocytosis, and vesicular transport regulation [48], also varied interindividually, and the VPS34 levels mainly remained stable or decreased following treatment with ER stress-modulating compounds (Fig. S11). Therefore, the induction of ER stress was associated with changes in the autophagic activity of the tested cells. Nevertheless, the direction and extent of the response were partly dependent on autophagy levels in the resting state and were partly isolate-specific.

Tunicamycin and the two copper complexes had negligible effects on cell viability and metabolism; only salubrinal induced a decrease in cell proliferation (Fig. 5G-H).

To evaluate the role of ER stress in the response of tumor cells to erastin, we treated a randomly selected set of eight isolates of tumor cells with TUDCA and erastin together and performed endpoint ATP measurements. The treatment lasted for 24 h, which is sufficient to observe the effects of erastin but insufficient to observe the relatively mild effects on cell proliferation induced by TUDCA. Among the eight tested isolates of tumor cells, only one responded to erastin treatment (tumor 16 N), and combined treatment with erastin and TUDCA did not affect the readout (Fig. S12).

In a set of six randomly selected isolates of tumor cells, we further tested whether the erastin and TUDCA treatments affected the levels of reactive oxygen species (assessed by CM-H_2DCFDA), mitochondrial superoxide (assessed by MitoSOX), and intracellular reduced glutathione (assessed by ThiolTracker), and compared the obtained data with endpoint ATP (CellTiter-Glo) measurements. While the total ROS levels remained nearly stable, there were prominent decreases in mitochondrial superoxide and intracellular reduced glutathione levels in five of the six tested isolates of tumor cells following erastin treatment. These changes were independent of glucose levels in the cell culture medium. Surprisingly, TUDCA treatment did not rescue the erastin-induced changes in mitochondrial superoxide or intracellular reduced glutathione (Fig. S13).

Susceptibility of tumor cell isolates to compounds that regulate the metabolism of amino acids and fatty acids

Given that HGSOC is challenging to target, we tested a panel of compounds that modulate the metabolism of amino acids and fatty acids and their synthetic lethal effects in combination with glucose or glutamine withdrawal (Fig. 6). This approach identified several promising candidates, which should be addressed in detail in

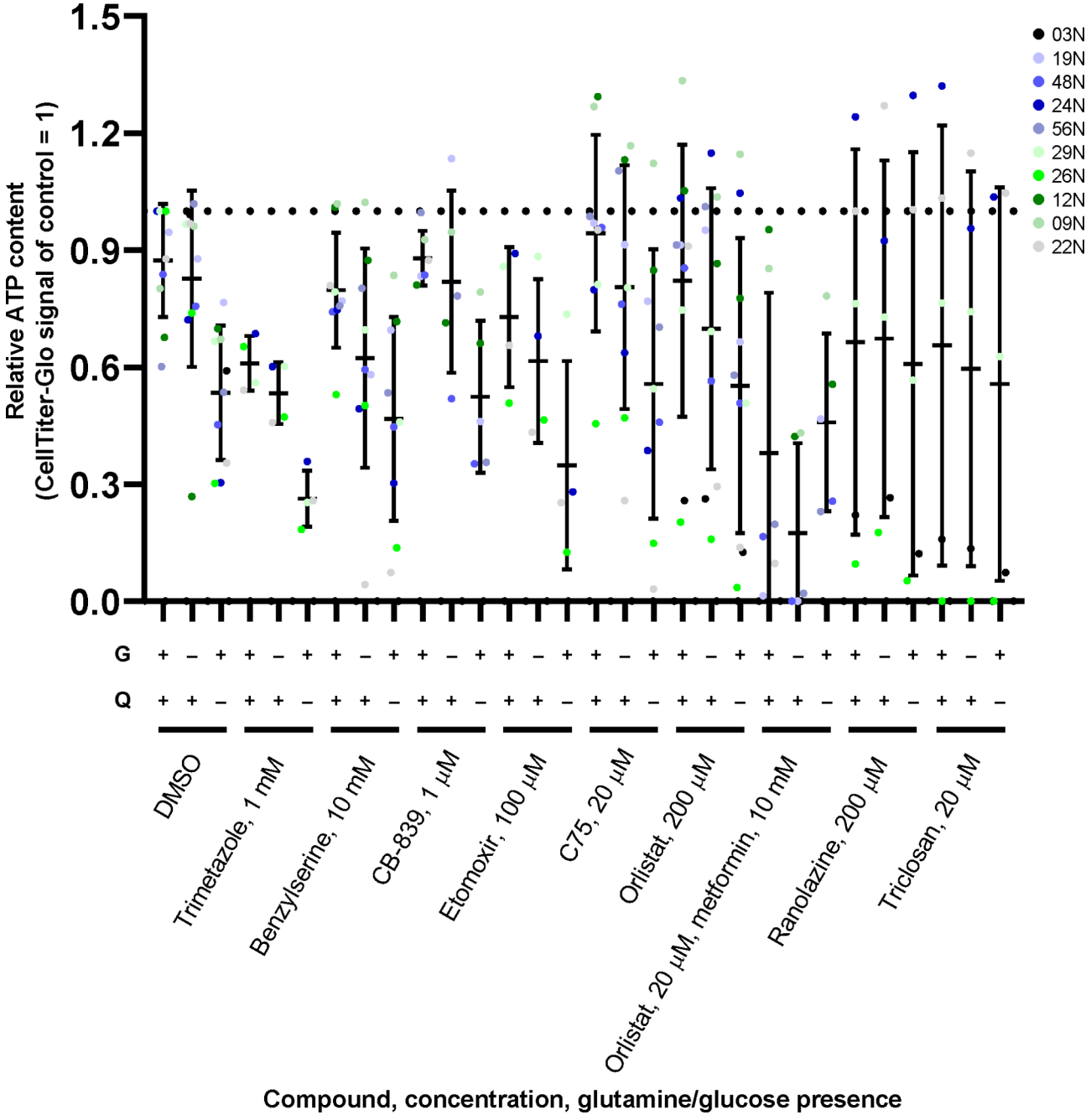

Fig. 6 Susceptibility of tumor cell isolates to compounds that regulate the metabolism of amino acids and fatty acids. The cellular ATP levels in tumor cells following treatment with compounds that affect cellular metabolism were measured by the CellTiter-Glo cell viability assay. The study compounds included trimetazole (1 mM), benzylserine (10 mM), CB-839 (1 μM), etomoxir (100 μM), C75 (20 μM), orlistat (200 μM), a combination of orlistat with metformin (10 mM), ranolazine (200 μM), and triclosan (20 μM). The cells were cultivated in a complete medium (+Q, +G) or medium with depleted glucose or glutamine; the presence or absence of glucose and glutamine in the medium is indicated on the X axis. Individual data points represent the means of four measurements from each patient-derived cell isolate and are shown relative to those of the isolates in complete (control) medium (+Q, +G) without the study compound. Color codes indicate individual tumor cell isolates. The bars indicate the means and SDs

future studies. These include the synergistic effects of the OCT2 inhibitor trimetazole or a fatty acid oxidation inhibitor with glutamine deprivation. In a glucose-depleted medium, the most promising results were observed with orlistat combined with metformin. The responses of individual tumor cell isolates were highly heterogeneous. However, the extent of response of the respective individual tumor cell isolate was often similar across multiple compounds (see color codes in Fig. 6). Therefore, to address drug sensitivity and specificity of

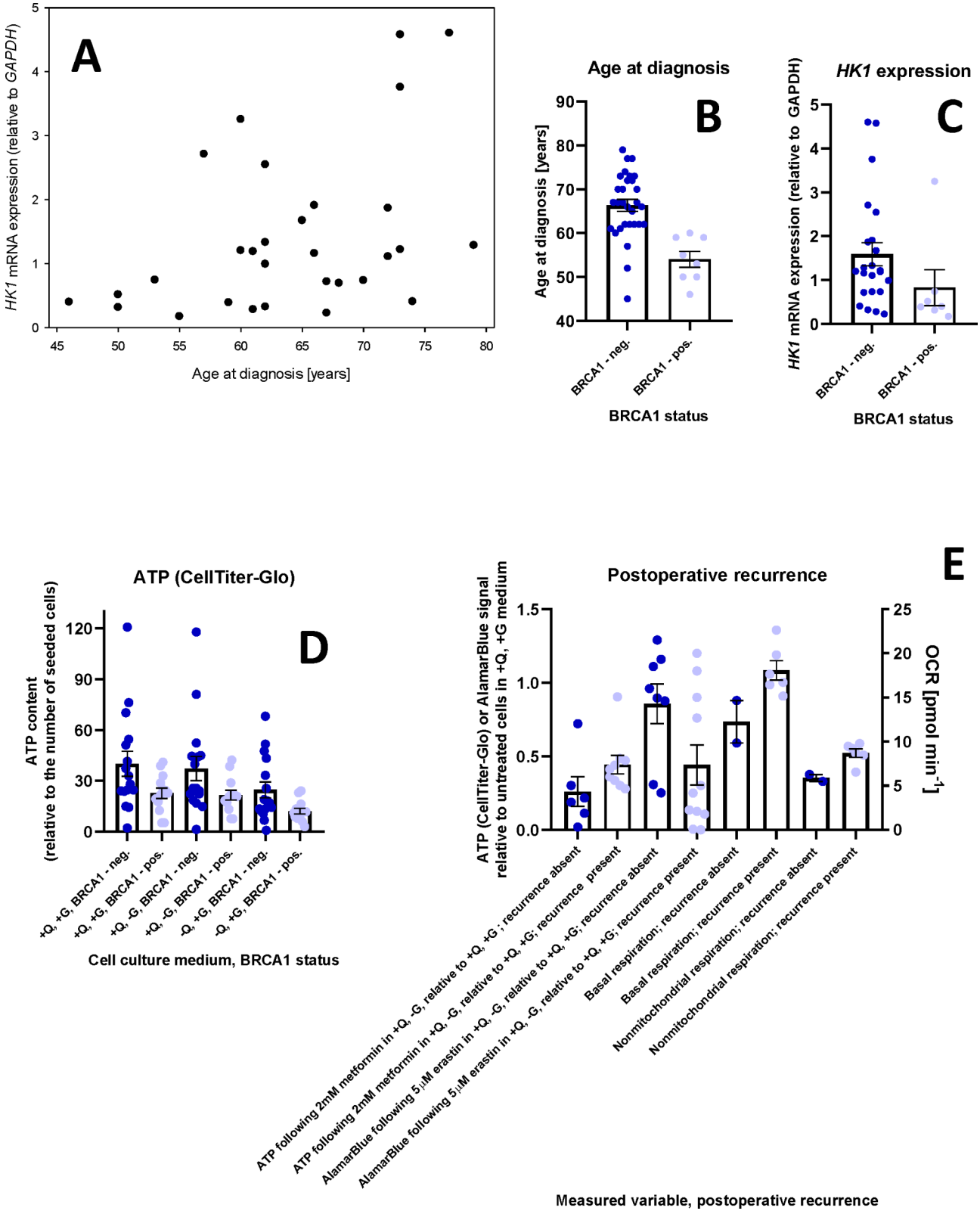

Fig. 7 (See legend on next page.)

(See figure on previous page.)

Fig. 7 Relationships between metabolic parameters of the tumor cells and clinical parameters of matched patients. (**A**) Levels of *HK1* transcripts (relative to *GAPDH*) in tumor cell isolates plotted against the age at diagnosis of their source patients. (**B**) Age at diagnosis in patients with HGSOC stratified according to the presence of cancer-associated variations in BRCA1. (**C**) Levels of *HK1* transcripts (relative to *GAPDH*) in tumor cell isolates stratified according to the presence of cancer-associated variations in BRCA1. (**D**) Proliferation of tumor cell isolates in complete media, and media without glutamine or glucose; the isolates were stratified according to the presence of macroscopic postoperative residua. (**E**) Changes in ATP levels following metformin treatment in a glucose-deficient medium as measured using CellTiter-Glo, changes in alamarBlue signal following erastin treatment in glucose-deficient medium, basal respiration, and nonmitochondrial respiration as measured using OCR in tumor cell isolates stratified according to the presence of postoperative recurrence

compounds targeting the metabolism of amino acids and fatty acids in patients with HGSOC requires individualized precision medicine approaches.

Tumor cells were inhibited by treatment with the OCT2 transporter inhibitor trimetazole (1 mM), and this effect was synergistic with glutamine deprivation (Fig. 6). The response to trimetazole alone was uniform; the ATP concentration, a proxy of the cell count, decreased to only 61.0%±3.0% of the control level following trimetazole treatment, and the synthetic lethal effects of trimetazole combined with glutamine deprivation induced a further decrease to 26.3%±3.1% of the control level (Fig. 6).

With respect to the metabolism of amino acids, benzylserine (10 mM), an inhibitor of leucine and glutamine uptake, induced heterogeneous responses in the tested tumor cell isolates, with most of the tested tumor cells responding only weakly to this treatment. Interestingly, when benzylserine was combined with glucose deprivation, the ATP concentration decreased to 62.3%±8.8%, and when benzylserine was combined with glutamine deprivation, the ATP concentration decreased to 46.7%±8.2%. Similarly, the glutaminase inhibitor CB-839 (1 μM) induced only a weak response when the cells were grown in complete medium (87.9%±2.6%). When CB-839 was combined with glucose deprivation, the ATP level decreased to 81.9%±9.3% of the control level. When CB-839 was combined with glutamine deprivation, the ATP level further decreased to only 52.4%±7.8% of the control level (Fig. 6).

We further tested the effects of these two compounds on the metabolism of amino acids in combination with TUDCA to determine whether reducing ER stress has the potential to affect treatment outcomes. TUDCA treatment did not rescue the benzylserine-induced (Fig. S14) or CB-839-induced (Fig. S13) changes. We further found that despite CB-839 having strong effects on relative ATP levels in both glucose- and glutamine-deprived media, this compound had negligible effects on total ROS, mitochondrial superoxide, and intracellular reduced glutathione (Fig. S13).

With respect to lipid metabolism, the most prominent effects were obtained when the fatty acid oxidation inhibitor etomoxir (100 μM) was used. When etomoxir was used alone, the ATP level was reduced to 72.8%±7.8% of the control level. When etomoxir was combined with glucose deprivation, the ATP concentration decreased to 61.5%±9.1%. When combined with glutamine deprivation, the ATP concentration further decreased to 34.9%±11.5% of the control level (Fig. 6). The responses to the FASN inhibitor C75 (20 μM) and the lipase inhibitor orlistat (200 μM) were in a similar direction but much weaker. Interestingly, the combination of orlistat with metformin (10 mM) induced a highly variable response when applied to cells in complete medium and strongly inhibited cells cultured in glucose-depleted medium. The ATP level in cells derived from the two tested tumor cell isolates and cultured in complete medium decreased to only 85% and 95% of that of the control but decreased to less than 20% of that of the control in the other cell isolates. In glucose-depleted medium, the ATP level decreased to 17.1%±9.4% of the control level. In glutamine-depleted medium, the decrease was much milder. The ATP levels were 45.8%±9.1% of the control level (Fig. 6). Ranolazine (200 μM) serves as a partial fatty acid oxidation inhibitor and an inhibitor of sodium channels and is thus a calcium uptake inhibitor; this compound induced highly variable responses, which were unaffected by glucose or glutamine deprivation, in the tested tumor cells. A similar direction and heterogeneity of responses were observed with the mild mitochondrial uncoupler triclosan (20 μM) (Fig. 6).

Correlation with clinical parameters

As the examined cohort of patients with HGSOC was relatively heterogeneous (see Table S1 for more details), we examined the correlations of the examined cellular metabolism parameters of the tumor cells with the clinical parameters of the patients, classification of the examined tumors, and applied treatments and treatment outcomes. Approximately one-quarter of the examined patients were <60 years of age (mean±SD 64±9 years). Age at diagnosis was independent of all the analyzed parameters except for the levels of *HK1* transcripts (Spearman *rho*=0.39; $p=0.03$; Fig. 7A). All the examined tumors were of the serous histotype of grade III but differed in their FIGO substages. FIGO substage was inversely correlated with the abundance of *IDO1* (Spearman *rho* = -0.43; $p=0.017$) and *FABP4* transcripts (Spearman *rho* = -0.58; $p=0.018$), and inversely correlated with the cell proliferation following TUDCA treatment (Spearman *rho* = -0.62; $p=0.048$).

Over one-fifth of the patients were positive for germinal cancer-associated variations in BRCA1 or BRCA2; several additional patients were positive for somatic mutations in these proteins only. As expected, the presence of cancer-associated variations in BRCA1 was inversely correlated with age at diagnosis (Spearman *rho* = -0.61; $p<0.001$; Fig. 7B) and inversely correlated with the levels of *TBP* (Spearman *rho* = -0.79; $p=0.025$) and *HK1* (Spearman *rho* = -0.37; $p=0.039$; Fig. 7C) transcripts.

Two-fifths of the patients were treated with neoadjuvant chemotherapy. These patients were at significantly higher FIGO substages (Spearman *rho*=0.34; $p=0.029$), but the application of neoadjuvant chemotherapy was not associated with changes in the properties of the obtained tumor cells. Approximately two-fifths of the patients had macroscopic postoperative residua; these patients were, as expected, at a higher FIGO stage (Spearman *rho*=0.45; $p=0.005$), and isolates from these patients had a surprisingly lower ability to proliferate in media without glutamine (Spearman *rho* = -0.41; $p=0.026$) or glucose (Spearman *rho* = -0.39; $p=0.037$) but did not differ in their ability to proliferate in complete media (Spearman $p>0.05$) (Fig. 7D).

Postoperative recurrence was common and reached 59% within three years following tumor resection (47% in patients with R0, 62% in patients with R2; Table S1). As expected, postoperative recurrence was inversely correlated with the use of PARPi (Spearman *rho* = -0.61; $p<0.001$) and consequently with the presence of cancer-associated mutations in BRCA1 (Spearman *rho* = -0.38; $p=0.026$) or BRCA2 (Spearman *rho* = -0.44; $p=0.010$). Interestingly, postoperative recurrence was also positively correlated with greater basal and nonmitochondrial respiration, as measured by the OCR (Spearman *rho*=0.75; $p=0.021$, both; Fig. 7E), and with cell proliferation following metformin treatment in glucose-deficient medium (Spearman *rho* = -0.54; $p=0.038$; Fig. 7E). Concerning changes in alamarBlue signal following erastin treatment in glucose-deficient medium, the tumor cells formed two groups (responders and nonresponders). The responders were more commonly isolated from patients with postoperative recurrence (6 of 10 cases), whereas the nonresponders were more commonly isolated from patients without postoperative recurrence (7 of 9 cases) (Fig. 7E).

Limitations

The high variability of the examined patients should be considered a limitation of the present study. Besides the variability among tumor cell isolates, we observed similar variability even among ovarian fibroblast isolates. The variability in ovarian fibroblasts cannot be linked to cancer-associated changes. However, it may be linked to the age-related loss of ovarian function (all examined patients were middle-aged or older). Owing to the enormous metabolic heterogeneity of tumor cells and ovarian fibroblasts, treatment efficacy is difficult to predict with any of the markers used in this or previous studies.

Another limitation is the focus on cells cultivated ex vivo in 2D conditions. This study revealed that treatment outcomes varied dramatically with changing glucose or glutamine concentrations. Sensitivity to cell culture media composition is directly relevant to the intratumoral environment, where nutrients are often limiting, and glucose is typically a poorly available nutrient. Studies of 3D organoids are needed to corroborate the obtained data. Notably, all the tumor cell isolates partly changed their phenotype during the first weeks of cultivation before their use in the experiments described above. The cells initially contained large lipid droplets, which were lost during cultivation, and consequently, the analyzed cells did not contain lipid droplets.

On the basis of the present study settings, we cannot rule out the role of differences in intrinsically produced glutamate. There was no glutamate in the DMEM provided to the cells (Thermo Fisher #A14430), and glutamine was added or not added, as indicated. On the basis of our metabolomic experiments with ovarian cancer cell lines [35], we assume that glutamate is abundantly present and secreted in the cell culture medium during cell cultivation. However, its levels may vary depending on the cultivation conditions and the cell isolate used.

Conclusions

We provided conclusive evidence that the previously proposed existence of two distinct groups of HGSOC cells with high and low OXPHOS metabolism that are associated with the responses to glucose and glutamine withdrawal does not accurately describe the situation in tumor cells. Tumor cells formed a continuum of OXPHOS phenotypes. Surprisingly, the responses of tumor cells to glutamine or glucose withdrawal were only partially related to the expression levels of ETC proteins, and the associations between ETC proteins and the OCR or ECAR were particularly weak. The regulation of OXPHOS metabolism in tumor cells is complex, and its prediction in individual patients is challenging. Identification and modulation of the OXPHOS status of HGSOC cells is important, as HGSOC cells that prioritize OXPHOS demonstrate better responses to paclitaxel and carboplatin [4]. However, as we have shown here in cells isolated from chemotherapy-treated and chemotherapy-naïve patients, the HGSOC cells exhibited multiple metabolic profiles. These cells differed in their sensitivity to glucose or glutamine withdrawal, and their growth under glutamine-deficient conditions was negatively correlated with *HK2* expression but not *HK1* expression. Notably, *HK2* expression is increased in most tumors,

whereas *HK1* is highly expressed in HGSOC (particularly BRCA1-negative HGSOC) and a few other tumor types, which suggests a specific regulatory role for *HK2* in HGSOC. All the analyzed HGSOC tumors and tumor cells exhibited increased ER stress. The incubation of tumor cells with compounds that relieve ER stress stimulated faster proliferation. In contrast, it was possible to further increase the level of ER stress by incubating the cells with tunicamycin. However, the use of copper(II)-phenanthroline complexes, which were recently proposed to be alternative ER stress inducers on the basis of experiments in OC cell lines [13], did not affect BiP levels in tumor cells or ovarian fibroblasts. Notably, treatment with tunicamycin or copper(II)-phenanthroline complexes had negligible effects on cell viability and metabolism. The compounds that induce or suppress ER stress only modulated the autophagic responses of the cells, but the responses varied individually based on the autophagic status of the respective HGSOC cell isolates before treatment. Tumor cells remain a difficult-to-treat target, and tumor cell metabolism cannot be stratified into two groups on the basis of OXPHOS activity. Instead, tumor cells form a continuum of metabolic phenotypes with a broad range of protein expression patterns. Caution is needed when interpreting data obtained from established immortalized HGSOC cell lines, as most of these cell lines are glucose-addicted due to long-term cultivation in glucose-rich media.

Abbreviations

C0	$[Cu(phen)_2(OH_2)](ClO_4)_2$
C1	$[Cu(phen)_2(2\text{-imidazolidinethione})](ClO_4)_2$
ECAR	Extracellular acidification rate
ER	Endoplasmic reticulum
ETC	Electron transport chain
HGSOC	High-grade serous ovarian carcinoma
OC	Ovarian carcinoma
OCR	Oxygen consumption rate
OXPHOS	Oxidative phosphorylation
TUDCA	Tauroursodeoxycholic acid
UPR	Unfolded protein response

Supplementary Information

The online version contains supplementary material available at https://doi.org/10.1186/s40170-024-00355-1.

Supplementary Material 1

Supplementary Material 2

Acknowledgements
Not applicable.

Author contributions
DS, LM, DG, KH, TPe, and PH performed the experiments. MHr and LR were responsible for the collection of clinical specimens. MHe was responsible for the pathological examination. TPi and JS were responsible for the materials and instrumentation. DS, KH, PV, and PH conceived and designed the experiments. PH analyzed the data, wrote the paper, and is responsible for the integrity of this work. All authors revised the article's intellectual content and approved the final version.

Funding
DS, DG, and PH have been funded by the Charles University in Prague project GA UK 324421. LM was funded by the Czech Health Research Council project NU21-03-00539. LM and PV were funded by the Masaryk University project MUNI/A/1598/2023. KH and JS were funded by the European Union – Next Generation EU – program No. LX22NPO5102.

Data availability
All the data are available in the main text or in the supplementary materials.

Declarations

Ethics approval and consent to participate
The use of primary cells was approved by the Ethics Committee of the Third Faculty of Medicine, Charles University (approval not numbered, dated April 29, 2020) and by the Ethics Committee of the University Hospital Královské Vinohrady (approval #EK-VP/24/0/2020, dated June 3, 2020). Written informed consent was obtained from each donor of primary cells.

Consent for publication
Not applicable.

Competing interests
DS, DG, and PH were funded by the Charles University in Prague project GA UK 324421. LM was funded by the Czech Health Research Council project NU21-03-00539. LM and PV were funded by the Masaryk University project MUNI/A/1598/2023. KH and JS were funded by the European Union – Next Generation EU – program No. LX22NPO5102. The authors declare no other competing interests.

Author details
[1]Third Faculty of Medicine, Charles University, Ruská 87, Prague CZ-100 00, Czech Republic
[2]Department of Histology and Embryology, Faculty of Medicine, Masaryk University, Brno, Czech Republic
[3]Research Centre for Applied Molecular Oncology (RECAMO), Masaryk Memorial Cancer Institute, Brno, Czech Republic
[4]University Hospital Kralovské Vinohrady, Prague, Czech Republic
[5]Department of Pediatric Hematology and Oncology, Second Faculty of Medicine, CLIP – Childhood Leukaemia Investigation Prague, Charles University, Prague, Czech Republic
[6]Department of Chemical and Geological Sciences, University of Cagliari, Monserrato, CA, Italy
[7]First Department of Pathology, St. Anne's University Hospital, Brno, Czech Republic
[8]First Department of Pathology, Faculty of Medicine, Masaryk University, Brno, Czech Republic
[9]Motol University Hospital, Prague, Czech Republic
[10]International Clinical Research Center, St. Anne's University Hospital, Brno, Czech Republic

Received: 30 January 2024 / Accepted: 5 September 2024
Published online: 16 September 2024

References

1. George SH, Garcia R, Slomovitz BM. Ovarian cancer: the fallopian tube as the site of origin and opportunities for prevention. Front Oncol. 2016;6:108.
2. Sopik V, Iqbal J, Rosen B, Narod SA. Why have ovarian cancer mortality rates declined? Part I. Incidence. Gynecol Oncol. 2015;138:741–9.
3. Wright AA, Bohlke K, Armstrong DK, Bookman MA, Cliby WA, Coleman RL, et al. Neoadjuvant chemotherapy for newly diagnosed, advanced ovarian cancer: Society of Gynecologic Oncology and American Society of Clinical Oncology Clinical Practice Guideline. Gynecol Oncol. 2016;143:3–15.
4. Gentric G, Kieffer Y, Mieulet V, Goundiam O, Bonneau C, Nemati F, et al. PML-regulated mitochondrial metabolism enhances chemosensitivity in human ovarian cancers. Cell Metab. 2019;29:156–73.
5. Huang L-W, Lin C-Y, Lee C-C, Liu T-Z, Jeng C-J. Overexpression of GRP78 is associated with malignant transformation in epithelial ovarian tumors. Appl Immunohistochem Mol Morphol. 2012;20:381–5.

6. Samanta S, Tamura S, Dubeau L, Mhawech-Fauceglia P, Miyagi Y, Kato H, et al. Clinicopathological significance of endoplasmic reticulum stress proteins in ovarian carcinoma. Sci Rep. 2020;10:2160.
7. Pils D, Horak P, Vanhara P, Anees M, Petz M, Alfanz A, et al. Methylation status of TUSC3 is a prognostic factor in ovarian cancer. Cancer. 2013;119:946–54.
8. Kratochvilova K, Horak P, Esner M, Soucek K, Pils D, Anees M, et al. Tumor suppressor candidate 3 (TUSC3) prevents the epithelial-to-mesenchymal transition and inhibits tumor growth by modulating the endoplasmic reticulum stress response in ovarian cancer cells. Int J Cancer. 2015;137:1330–40.
9. Chen X, Cubillos-Ruiz JR. Endoplasmic reticulum stress signals in the tumour and its microrvironment. Nat Rev Cancer. 2021;21:71–88.
10. Huang N, Yu Y, Qiao J. Dual role for the unforlded protein response in the ovary: adaptation and apoptosis. Protein Cell. 2017;8:14–24.
11. Kyathanahalli C, Organ K, Moreci RS, Anamthathmakula P, Hassan SS, Caritis SN, et al. Uterine endoplasmic reticulum stress-unfolded protein response regulation of gestational length in caspase-3 and-7-dependent. Proc Natl Acad Sci USA. 2015;112:14090–5.
12. Chui MH, Doodnauth SA, Erdmann N, Tiedemann RE, Sircoulomb F, Drapkin R, et al. Chromosomal instability and mTORC1 activation through PTEN loss contribute to proteotoxic stress in ovarian carcinoma. Cancer Res. 2019;79:5536–49.
13. Moráň L, Pivetta T, Masuri S, Vašíčková K, Walter F, Prehn J, et al. Mixed copper(ii)-phenanthroline complexes induce cell death of ovarian cancer cells by evoking the unfolded protein response. Metallomics. 2019;11:1481–9.
14. Masuri S, Cadoni E, Cabiddu MG, Isaia F, Demuru MG, Moráň L, et al. The first copper(ii) complex with 1,10-phenanthroline and salubrinal with interesting biochemical properties. Metallomics. 2020;12:891–901.
15. Janczar S, Nautiyal J, Xiao Y, Curry E, Sun M, Zanini E, et al. WWOX sensitises ovarian cancer cells to paclitaxel via modulation of the ER stress response. Cell Death Dis. 2017;8:e2955.
16. Avril T, Vauléon E, Chevet E. Endoplasmic reticulum stress signaling and chemotherapy resistance in solid cancers. Oncogenesis. 2017;6:e373.
17. Notte A, Rebucci M, Fransolet M, Roegiers E, Genin M, Tellier C, et al. Taxol-induced unfolded protein response activation in breast cancer cells exposed to hypoxia: ATF4 activation regulates autophagy and inhibits apoptosis. Int J Biochem Cell Biol. 2015;62:1–14.
18. Mgaudat NM, Alali FQ, Matalqah SM, Matalka II, Jaradat SA, Al-Sawalha NA, et al. Inhibition of MEK sensitizes paclitaxel-induced apoptosis of human colorectal cancer cells by downregulation of GRP78. Anticancer Drugs. 2009;20:601–6.
19. Wilson AJ, Lalani AS, Wass E, Saskowski J, Khabele D. Romidepsin (FK228) comined with cisplatin stimulates DNA damage-induced cell death in ovarian cancer. Gynecol Oncol. 2012;127:579–86.
20. Du Y, Wu J, Zhang H, Li S, Sun H. Reduced expression of SIRT2 in serous ovarian carcinoma promotes cell proliferation through disinhibition of CDK4 expression. Mol Med Rep. 2017;15:1638–46.
21. Li W, Wang W, Dong H, Li Y, Li L, Han L, et al. Cisplatin-induced senescence in ovarian cancer cells is mediated by GRP78. Oncol Rep. 2014;31:2525–34.
22. Nacarelli T, Fukumoto T, Zunell JA, Fatkhutdinov N, Jean S, Cadungog MG, et al. NAMPT inhibition suppresses cancer stem-like cells associated with therapy-induced senescence in ovarian cancer. Cancer Res. 2020;80:890–900.
23. Xiao R, You L, Zhang L, Guo X, Guo E, Zhao F, et al. Inhibiting the IRE1α axis of the unfolded protein response enhances the antitumor effect of AZD1775 in TP53 mutant ovarian cancer. Adv Sci. 2022;9:e2105469.
24. Li X, Liu S, Chen X, Huang R, Ma L, Weng H, et al. GnRHa protects the ovarian reserve by reducing endoplasmic reticulum stress during cyclophosphamide-based chemotherapy. NJP Breast Cancer. 2021;7:132.
25. Moon H-S, Kim B, Gwak H, Sun DH, Song YS. Autophagy and protein kinase RNA-like endoplasmic reticulum kinase (PERK)/eukaryotic initiation factor 2 alpha kinase (eIF2α) pathway protect ovarian cancer cells from metformin-induced apoptosis. Mol Carcinog. 2016;55:346–56.
26. Shepherd TG, Thériault BL, Campbell EJ, Nachtigal MW. Primary culture of ovarian surface epithelial cells and ascites-derived ovarian cancer cells from patients. Nat Protoc. 2006;1:2643–9.
27. Pivetta T, Cannas MD, Demartin F, Castellano C, Vascellari S, Verani G, et al. Synthesis, structural characterization, formation constants and in vitro cytotoxicity of phenanthroline and imidazolidine-2-thione copper(II) complexes. J Inorg Biochem. 2011;105:329–38.
28. Wise DR, Thompson CB. Glutamine addiction: a new therapeutic target in cancer. Trends Biochem Sci. 2010;35:427–33.
29. Wise DR, DeBerardinis RJ, Mancuso A, Sayed N, Zhang X-Y, Pfeiffer HK, et al. Myc regulates a transcriptional program that stimulates mitochondrial glutaminolysis and leads to glutamine addiction. Proc Natl Acad Sci USA. 2008;105:18782–7.
30. Yuneva M, Zamboni N, Oefner P, Sachidanandam R, Lazebnik Y. Deficiency in glutamine but not glucose induces MYC-dependent apoptosis in human cells. J Cell Biol. 2007;178:93–105.
31. Pastò A, Pagotto A, Pilotto G, De Paoli A, De Salvo G, Baldoni A, et al. Resistance to glucose starvation as metabolic trait of platinum-resistant human epithelial ovarian cancer cells. Oncotarget. 2017;8:6433–45.
32. Dar S, Chhina J, Mert I, Chitale D, Buekers T, Kaur H, et al. Bioenergetic adaptations in chemoresistant ovarian cancer cells. Sci Rep. 2017;7:8760.
33. Hao J, Yan F, Zhang Y, Triplett A, Zhang Y, Schultz DA, et al. Expression of adipocyte/macrophage fatty acid-binding protein in tumor-associated macrophages promotes breast cancer progression. Cancer Res. 2018;78:2343–55.
34. Cui Y, Song M, Kim SY. Prognostic significance of fatty acid binding protein-4 in the invasive ductal carcinoma of the breast. Pathol Int. 2019;69:68–75.
35. Šimčíková D, Gardáš D, Hložková K, Hruda M, Žáček P, Rob L, et al. Loss of hexokinase 1 sensitizes ovarian cancer to high-dose metformin. Cancer Metab. 2021;9:41.
36. Furkan Alkan H, Walter KE, Luengo A, Madreiter-Sokolowski CT, Stryeck S, Lau AN, et al. Cytosolic aspartate availability determines cell survival when glutamine is limiting. Cell Metab. 2018;28:706–20.
37. He L, Wondisford FE. Metformin action: concentrations matter. Cell Metab. 2015;21:159–62.
38. Andrzejewski S, Gravel SP, Pollak M, St-Pierre J. Metformin directly acts on mitochondria to alter cellular bioenergetics. Cancer Metab. 2014;2:12.
39. Griss T, Vincent EE, Egnatchik R, Chen J, Ma EH, Faubert B, et al. Metformin antagonizes cancer cell proliferation by suppressing mitochondrial-dependent biosynthesis. PLoS Biol. 2015;13:e1002309.
40. Elia I, Haigis MC. Metabolites and the tumour microenvironment: from cellular mechanisms to systemic metabolism. Nat Metab. 2021;3:21–32.
41. Zhou H-H, Chen X, Cai L-Y, Nan X-W, Chen J-H, Chen X-X, et al. Erastin reverses ABCB1-mediated docetaxel resistance in ovarian cancer. Front Oncol. 2019;9:1398.
42. Battaglia AM, Sacco A, Perrotta ID, Faniello MC, Scalise M, Torella D, et al. Iron administration overcomes resistance to erastin-mediated ferroptosis in ovarian cancer cells. Front Oncol. 2022;12:868351.
43. Wang W, Kryczek I, Dostál L, Lin H, Tan L, Zhao L, et al. Effector T cells abrogate stroma-mediated chemoresistance in ovarian cancer. Cell. 2016;165:1092–105.
44. Bhattarai KR, Riaz TA, Kim H-R, Chae H-J. The aftermath of the interplay between the endoplasmic reticulum stress response and redox signaling. Exp Mol Med. 2021;53:151–67.
45. Pivetta T, Trudu F, Valletta E, Isaia F, Castellano C, Demartin F, et al. Novel copper(II) complexes as new promising antitumour agents. A crystal structure of $[Cu(1,10\text{-phenanthroline-}5,6\text{-dione})_2(OH_2)(OClO_3)](ClO_4)$. J Inorg Biochem. 2014;141:103–13.
46. Qi Z, Chen L. Endoplasmic reticulum stress and autophagy. Adv Exp Med Biol. 2019;1206:167–77.
47. Li Y, Chen Y. AMPK and autophagy. Adv Exp Med Biol. 2019;1206:85–108.
48. Liu Y, Yang Q, Chen S, Li Z, Fu L. Targeting VPS34 in autophagy: an update on pharmacological small-molecule compounds. Eur J Med Chem. 2023;256:115467.

Publisher's note